Maskless 2-Dimensional Digital Subtraction Angiography Generation Model for Abdominal Vasculature using Deep Learning

Maskless 2-Dimensional Digital Subtraction Angiography Generation Model for Abdominal Vasculature using Deep Learning

Hiroki Yonezawa, MD, Daiju Ueda, MD, PhD, Akira Yamamoto, MD, PhD, Ken Kageyama, MD, PhD, Shannon Leigh Walston, MS, Takehito Nota, MD, Kazuki Murai, MD, PhD, Satoyuki Ogawa, MD, PhD, Etsuji Sohgawa, MD, Atsushi Jogo, MD, PhD, Daijiro Kabata, MPH, and Yukio Miki, MD, PhD

ABSTRACT

Purpose: To develop a deep learning (DL) model to generate synthetic, 2-dimensional subtraction angiograms free of artifacts from native abdominal angiograms.

Materials and Methods: In this retrospective study, 2-dimensional digital subtraction angiography (2D-DSA) images and native angiograms were consecutively collected from July 2019 to March 2020. Images were divided into motion-free (training, validation, and motion-free test datasets) and motion-artifact (motion-artifact test dataset) sets. A total of 3,185, 393, 383, and 345 images from 87 patients (mean age, 71 years ± 10; 64 men and 23 women) were included in the training, validation, motion-free, and motion-artifact test datasets, respectively. Native angiograms and 2D-DSA image pairs were used to train and validate an image-to-image translation model to generate synthetic DL-based subtraction angiography (DLSA) images. DLSA images were quantitatively evaluated by the peak signal-to-noise ratio (PSNR) and structural similarity (SSIM) using the motion-free dataset and were qualitatively evaluated via visual assessments by radiologists with a numerical rating scale using the motion-artifact dataset.

Results: The DLSA images showed a mean PSNR (± standard deviation) of 43.05 dB ± 3.65 and mean SSIM of 0.98 ± 0.01, indicating high agreement with the original 2D-DSA images in the motion-free dataset. Qualitative visual evaluation by radiologists of the motion-artifact dataset showed that DLSA images contained fewer motion artifacts than 2D-DSA images. Additionally, DLSA images scored similar to or higher than 2D-DSA images for vascular visualization and clinical usefulness.

Conclusions: The developed DL model generated synthetic, motion-free subtraction images from abdominal angiograms with similar imaging characteristics to 2D-DSA images.

ABBREVIATIONS

DL = deep learning, DLSA = deep learning-based subtraction angiography, PSNR = peak signal-to-noise ratio, SSIM = structural similarity, 2D-DSA = 2-dimensional digital subtraction angiography

In many clinical scenarios that require angiography, 2-dimensional digital subtraction angiography (2D-DSA) is used as the primary imaging procedure because this technique provides clear imaging of blood vessels and requires only small amounts of contrast medium (1). A 2D-DSA image is created by subtracting a mask image from a native angiogram. A mask image is the background anatomical image that represents the image before the contrast agent reaches the vessel. The native angiogram is the real-time image and shows the vasculature with the contrast agent with the background anatomical image.

The primary limitation of 2D-DSA is motion artifacts, which are caused by a misalignment between the native angiogram and the mask image. The presence of motion artifacts makes it difficult to clearly identify vessels. Body movements, respiration, intestinal movement, and cardiac pulsatility can all cause motion artifacts. During image acquisition, patients are asked to remain as still as possible

Figures E1–E5, **Tables E1–E9**, and **Appendices A–D** can be found by accessing the online version of this article on *www.jvir.org* and selecting the Supplemental Material tab.

J Vasc Interv Radiol 2022; 33:845–851
https://doi.org/10.1016/j.jvir.2022.03.010

RESEARCH HIGHLIGHTS

- A deep learning-based subtraction angiography (DLSA) was developed that can create abdominal 2-dimensional digital subtraction angiography (DSA)–like images from only native angiograms without mask images.
- DLSA images showed a mean peak signal-to-noise ratio (± standard deviation) of 43.05 dB ± 3.65 and mean structural similarity of 0.98 ± 0.01, indicating high agreement with the original 2-dimensional DSA images, and had less motion artifact than the DSA.
- The DLSA model has the potential to achieve better testing, better treatment, use of less contrast agent, and less radiation exposure through artifact reduction during abdominal angiography.

and hold their breath to prevent motion artifacts. However, because of various physiological conditions, some patients may not be able to remain still during image acquisition. The presence of motion artifacts often requires reimaging, which necessitates that patients are exposed to additional contrast agent and radiation, as well as a longer period of time to treatment or testing.

Deep learning (DL), as a field of artificial intelligence, has received substantial attention in recent years (2) and has been integrated into various radiological applications (3,4). Image processing techniques such as remasking and pixel shifting are routinely employed to reduce the effects of patient motion (5,6). In recent years, maskless methods designed to overcome limitations from motion artifacts have also emerged. For example, previous studies (7–10) that have evaluated the cerebral region have proposed maskless angiography for both 2D-DSA and 3-dimensional digital subtraction angiography. Maskless models are ideal candidates for abdominal angiography because motion-caused artifacts are more common in the abdominal region.

In this study, a DL model was trained using abdominal angiograms and 2D-DSA images to generate synthetic DL-based subtraction angiography (DLSA) images. The model utilized was based on a previously developed DL model (9).

MATERIALS AND METHODS

Study Design

This retrospective study was approved by the Ethical Committee of Osaka City University Graduate School of Medicine. Because the images were acquired during daily clinical practice, the need for informed consent was waived. This study followed the Checklist for Artificial Intelligence in Medical Imaging and Standards for Reporting Diagnostic Accuracy statements (11,12). First, native angiograms and 2D-DSA images were retrospectively collected. The DL model was trained and tuned with pairs of native angiograms and 2D-DSA images without motion artifacts. The

STUDY DETAILS

Study type: Laboratory study

DLSA images generated from the trained model were quantitatively and qualitatively evaluated. In the quantitative evaluations, the DLSA images were evaluated by the peak signal-to-noise ratio (PSNR) and structural similarity (SSIM) compared with the original 2D-DSA images (13,14). In the qualitative visual evaluations, the DLSA images were compared with the original 2D-DSA images by 8 interventional radiologists across 3 different imaging characteristics.

Data Collection

All abdominal angiograms were collected consecutively at 1 facility between July 2019 and March 2020, and no exclusion criteria were adopted. All images were collected using a C-arm cone-beam 2D-DSA system (Artis Zee BA Twin; Siemens Healthineers, Erlangen, Germany). Although the method of contrast agent administration varied depending on the arteries, typical examples are shown in **Appendix A** (available online on the article's Supplemental Material page at *www.jvir.org*). Both 2D-DSA images with automatic pixel shifting and native angiograms were collected. If more than 1 sequence was performed for a patient, all the images in every sequence were collected.

Ground Truth Labeling

Each 2D-DSA image was classified by the authors, 2 radiologists (H.Y., D.U.) with 6 and 5 years of experience in interventional radiology, into groups with and without motion artifacts on a sequence basis as follows: (*a*) category 1, no artifacts; (*b*) category 2, slight artifacts; (*c*) category 3, some artifacts and reimaging recommended; and (*d*) category 4, strong artifacts and reimaging needed. In the event of disagreement, consensus was achieved by discussion. Categories 1 and 2 were classified as angiograms without motion artifacts. Categories 3 and 4 were classified as angiograms with motion artifacts. Detailed categorization is described in **Figure E1** and **Appendix B** (available online at *www.jvir.org*).

Image Processing

The images were first resized such that the long side of an image was 256 pixels, maintaining the aspect ratio of the image. The short side of an image was then padded with black to 256 pixels.

Data Partitioning

A total of 4 datasets were prepared: (*a*) training, (*b*) validation, (*c*) motion-free test, and (*d*) motion-artifact test

datasets. To train and evaluate the model, native angiograms and 2D-DSA images with the same time point, from the same patient, were paired on an image-by-image basis. Paired images with motion artifacts formed the motion-artifact test dataset. Paired images without motion artifacts were first randomly divided into training, validation, and motion-free test datasets at a ratio of 8:1:1, split patient-wise. This partition was performed on a per-patient basis to prevent the overlapping of images between the datasets.

Data Characteristics

In total, 4,306 paired images were collected from 120 sequences in 87 patients (mean age, 71 years ± 10; 64 men and 23 women). The training dataset comprised 3,185 paired images in 88 sequences from 64 patients (mean age, 71 years ± 11; 45 men and 19 women), the validation dataset contained 393 paired images in 11 sequences from 8 patients (mean age, 72 years ± 8; 8 men), the motion-free test dataset comprised 383 paired images in 11 sequences from 9 patients (mean age, 72 years ± 5; 7 men and 2 women), and the motion-artifact test dataset contained 345 paired images in 10 sequences from 6 patients (mean age, 69 years ± 12; 4 men and 2 women). Detailed demographic information of the datasets is provided in **Table 1**. The classification of motion artifacts for the datasets is shown in **Table E1** (available online at *www.jvir.org*). Disagreements between the radiologists regarding the presence of motion artifacts are shown in **Table E2** (available online at *www.jvir.org*).

Table 1. Demographics of the Datasets

Parameter	Training dataset	Validation dataset	Motion-free test dataset	Motion-artifact test dataset
Patients, n	64	8	9	6
Sequences, n	88	11	11	10
Paired images, n	3,185	393	383	345
Images by location, n				
Celiac artery	1,790	211	306	204
Common hepatic artery	788	106	33	35
Superior mesenteric artery	607	76	44	106
Patients by disease, n				
HCC	49	7	7	3
Rupture	0	0	0	1
Liver injury	2	0	0	1
Liver metastasis	3	0	0	0
Gastrointestinal bleeding	5	0	0	2
Intra-abdominal bleeding	3	1	0	0
Cholangiocellular carcinoma	2	0	0	0
Pancreatic cancer	0	0	1	0
Abscess	0	0	1	0

HCC = hepatocellular carcinoma.

Model Development

Usually, 2D-DSA images are generated by subtracting a mask image from a native angiogram. If a DL model could be trained to extract features related to the background, the model may be capable of replacing the need for a mask; this concept was the basis for the development of the model.

To implement background extraction, it was necessary to train the DL model on the relationship between the native angiogram and the 2D-DSA image without motion artifacts. When 2D-DSA images are acquired on a patient in motion, motion artifacts occur because there is a misalignment between the native angiogram and the mask image. However, with DL-based subtraction, the background can be removed from the native angiogram without using the mask image; therefore there is no misalignment. Thus, this model was trained on the basis of native angiograms and 2D-DSA images without motion artifacts.

The difference between the images generated by the model (DLSA) and the 2D-DSA images was expressed as a loss value, and the model with the lowest loss value across all the images in the dataset was considered as the highest performing model. The DL model was developed on the basis of pix2pix (15), a generative adversarial network, which is an image-to-image translation artificial intelligence model that uses paired images in the training and validation datasets. In the DL model, the generator adopted a U-Net–based architecture (16) and the discriminator adopted a convolutional PatchGAN classifier (17). The details of the developed DL model are shown in **Figure E2** and **Appendices C** and **D** (available online at *www.jvir.org*), and the source code is available online (18).

The model was trained with the training dataset and tuned with the validation dataset. The entire network was used for pixel-by-pixel regression and end-to-end mapping. The number of epochs was 100. The highest performing model was adopted when the sum of generator loss and L1 loss reached a minimum for the validation dataset. These models were built in PyTorch (19).

Quantitative Evaluation

Quantitative evaluation was performed on the validation and motion-free test datasets. The highest performing DL model was applied to these datasets, and the similarity between the DLSA image and the original 2D-DSA image was evaluated with the PSNR and SSIM (14). As shown in **Figure E3** (available online at *www.jvir.org*), PSNR is a traditional measurement of the average values of the differences in pixels between images, whereas SSIM is a measurement that takes into account not only the

differences in pixel values between images but also the differences in contrast and structure.

Qualitative Visual Evaluation

For images with motion artifacts, DLSA images cannot be quantitatively evaluated by comparison with 2D-DSA images because 2D-DSA images with motion artifacts are unsuitable as reference standards. Thus, the motion-artifact test dataset was assessed using qualitative visual evaluation.

The study protocol was as follows. To generate DLSA images, the highest performing model was applied to the native angiograms in the motion-artifact test dataset. A native angiogram, the original 2D-DSA image, and a DLSA image were arranged side by side; the placement of the 2D-DSA and DLSA images was randomized and blinded for the readers. The images were then compared and evaluated by 8 interventional radiologists (reader 1, 22 years of experience; reader 2, 16 years of experience; reader 3, 16 years of experience; reader 4, 15 years of experience; reader 5, 7 years of experience; reader 6, 6 years of experience; reader 7, 6 years of experience; and reader 8, 4 years of experience). Three types of visual evaluation were performed per sequence. The first test was a vascular visualization test to visually assess, per sequence, how well the DLSA images showed the arteries compared with the 2D-DSA images. The readers assessed all the main arteries and their branches contrasted in the images. Second, an artifact-reduction test was performed to visually assess how much the motion artifacts were reduced across the background region. Third, a clinical usefulness test was performed to visually assess how useful the DLSA images would be in guiding a procedure compared with the 2D-DSA images.

After the tests, the image pairs were divided into 5 classes on the basis of a score from 1 (2D-DSA images scored much higher than DLSA images) to 5 (DLSA images scored much higher than 2D-DSA images). A detailed description of each of the visual evaluation score is shown in **Table E3** (available online at *www.jvir.org*). Clinical information of the patients was not available to readers.

A diagnostic monitor (Eizo monitor, Eizo Flexscan RX560; Eizo, Ishikawa, Japan) was used to evaluate the 350 ppi images. There was no overlap between the radiologists who annotated the ground truth and those who performed the visual evaluation test. In addition to these tests to the motion-artifact test dataset, the motion-free test dataset was also visually evaluated using the same process.

Statistical Analysis

In quantitative evaluations, PSNR and SSIM, as 2 common measures of similarity in engineering image evaluation, were used to assess image quality. A linear mixed-effects model was used to compare the PSNR and SSIM between the imaging locations. A random slope and random intercept for each patient were taken into account because the datasets included some repeated measurements of a single patient. These statistical inferences were performed with a 2-sided 5% significance level. In visual evaluations, the grading of the visual ratings in the vascular visualization, artifact-reduction, and clinical usefulness tests were summarized, and the mean and standard deviations were assessed. All evaluations were analyzed by region. An author (D.K.) performed all analyses using R (version 4.0.3, 2020; R Foundation for Statistical Computing, Vienna, Austria) (20).

RESULTS

Model Development

The DL model was developed with the training dataset and tuned with the validation dataset. For the solver, the Adam optimizer (21), with a learning rate of 0.0002 and momentum parameters $\beta1 = 0.5$ and $\beta2 = 0.999$, was employed. The model was trained for 100 epochs using the training dataset while monitoring the loss value using the validation dataset. During this period, the lowest total loss value was 1.119 at 90 epochs. Therefore, the parameters at this epoch were adopted as the highest performing model. The learning curves for the DL model are shown in **Figure E4** (available online at *www.jvir.org*).

Quantitative Evaluation

For the quantitative evaluation of the DLSA images, the mean PSNR and SSIM (± standard deviation) were 44.10 dB ± 2.89 and 0.98 ± 0.01, respectively, in the validation dataset and 43.05 dB ± 3.65 and 0.98 ± 0.01, respectively in the motion-free test dataset. These results are presented in **Table 2**. The examples of the DLSA images in the motion-free test dataset are shown in **Figure 1** and **Figure E5** (available online at *www.jvir.org*).

Qualitative Visual Evaluation

For the visual evaluation of DLSA images in the motion-artifact test dataset, the mean score (± standard deviation) in the artifact-reduction test was 3.6 ± 1.1 (out of 5), with the DLSA images having fewer artifacts than the 2D-DSA images in all sequences. Moreover, the mean score in the vascular visualization test was 3.1 ± 0.9 (out of 5), and the mean score in the clinical usefulness test was 3.1 ± 1.0 (out of 5), with equal to superior vascular visualization and clinical usefulness.

Detailed data for each test on a sequence basis are shown in **Tables E4–E6** (available online at *www.jvir.org*). The examples of the DLSA images in the motion-artifact test dataset are shown in **Figures 2** and **3**. A sequence of images generated by the model, which were visually evaluated to be more clinically useful with reduced artifacts than the 2D-DSA images, is shown in **Video 1** (available online at *www.jvir.org*). The visual evaluations for the motion-free

Table 2. Quantitative Evaluation by PSNR and SSIM

Parameter	Mean	95% confidence interval		Global *P* value
		Lower	Upper	
PSNR				
Validation dataset				
Total (dB)	44.10 ± 2.89	NA	NA	NA
Location estimated mean value				
Celiac artery	43.644	42.241	45.047	<.001
Common hepatic artery	45.181	43.677	46.685	<.001
Superior mesenteric artery	46.227	44.402	48.051	<.001
Motion-free test dataset				
Total (dB)	43.05 ± 3.65	NA	NA	NA
Location estimated mean value				
Celiac artery	42.826	41.718	43.934	<.001
Common hepatic artery	45.264	43.172	47.356	<.001
Superior mesenteric artery	45.403	43.434	47.373	<.001
SSIM				
Validation dataset				
Total (dB)	0.98 ± 0.01	NA	NA	NA
Location estimated mean value				
Celiac artery	0.977	0.972	0.982	<.001
Common hepatic artery	0.982	0.977	0.988	<.001
Superior mesenteric artery	0.986	0.979	0.992	<.001
Motion-free test dataset				
Total (dB)	0.98 ± 0.01	NA	NA	NA
Location estimated mean value				
Celiac artery	0.997	0.973	0.980	.011
Common hepatic artery	0.983	0.977	0.989	.011
Superior mesenteric artery	0.975	0.969	0.981	.011

Note–Data are reported as mean ± standard deviation.
NA = not applicable; PSNR = peak signal-to-noise ratio; SSIM = structural similarity.

test dataset are available in **Tables E7–E9** (available online at *www.jvir.org*).

DISCUSSION

A DL model was developed to create synthetic subtraction angiograms (DLSA images) from native angiograms without subtracting mask images. In the quantitative analysis of the DLSA images, the mean PSNR and SSIM (± standard deviation) were 44.10 dB ± 2.89 and 0.98 ± 0.01, respectively, in the validation dataset and 43.05 dB ± 3.65 and 0.98 ± 0.01, respectively, in the motion-free test dataset, indicating that the DLSA images were highly similar to the original 2D-DSA images without motion artifacts. Visual evaluation by radiologists of the motion-artifact test dataset showed that the DLSA images contained fewer motion artifacts than the 2D-DSA images and had equal to superior vascular visualization and clinical usefulness.

In the field of abdominal angiography, 2D-DSA is indispensable but prone to motion artifacts. For decades, a variety of technologies have been used to address this problem (5). Approaches to capture images such as mask image modification (remasking), parallel shifting of native angiograms (pixel shifting processing), and automatic pixel shifting have been developed to reduce motion artifacts caused by body movements in 2D-DSA (5,22). Matrix pixel shifting is sometimes used as well. However, the model described in this study would enable the development of synthetic images much faster because it takes only a few seconds to apply the model to 1 sequence. As long as mask images are used for subtraction to make 2D-DSA images, motion artifacts will arise to some degree. However, this approach—based on previous study (9)—used only native angiograms to generate DLSA images. In this regard, the developed DL model could be used to generate images with fewer motion artifacts.

The developed DL model has the potential to allow interventional radiologists to provide optimized care to patients through the provision of angiograms with fewer artifacts, even if the patient moves during angiography. In clinical practice, visual evaluation of the DLSA images by interventional radiologists will be necessary to determine if these images could be used to overcome motion artifacts that are commonly encountered on 2D-DSA images. Interventional radiologists qualitatively scored DLSA images similar to or higher than 2D-DSA images (scores of 1–5, with a score of 3 indicating that the DLSA and 2D-DSA images were similar) for the reduction of motion artifacts (3.6 ± 1.1), vascular visualization (3.1 ± 0.9), and clinical usefulness (3.1 ± 1.0). Sequences with artifacts (images that are not clinically useful and may require reimaging) accounted for approximately 8% (345 of 4,306) of the sequences collected; therefore, contrast agent use and radiation exposure could be reduced by approximately 8% with the use of this model if reimaging were not required.

When the DLSA images were evaluated in detail, some artifacts were encountered, and evaluations of these images scored lower in both qualitative and visually qualitative analyses. **Figures 2** and **3** show angiograms in different sequences of the same examination in the motion-artifact test dataset. **Figure 2**, which shows an image that received a high evaluation, has a narrow angle of view, whereas **Figure 3**, which shows an image that received a low evaluation, has a wide angle of view. DLSA images with a wide angle of view tended to leave more artifacts than images with a narrower angle of view. This result may be because images with a wide angle of view include regions such as the iliac and femoral bones, for which a relatively small training dataset was available. Therefore, the use of images with a narrower angle of view for model training may improve the performance of the DL model.

There are some limitations of this study. All datasets were collected from a single institution and imaged with a single device. The PSNR and SSIM were relatively low in the region of the superior mesenteric artery because of

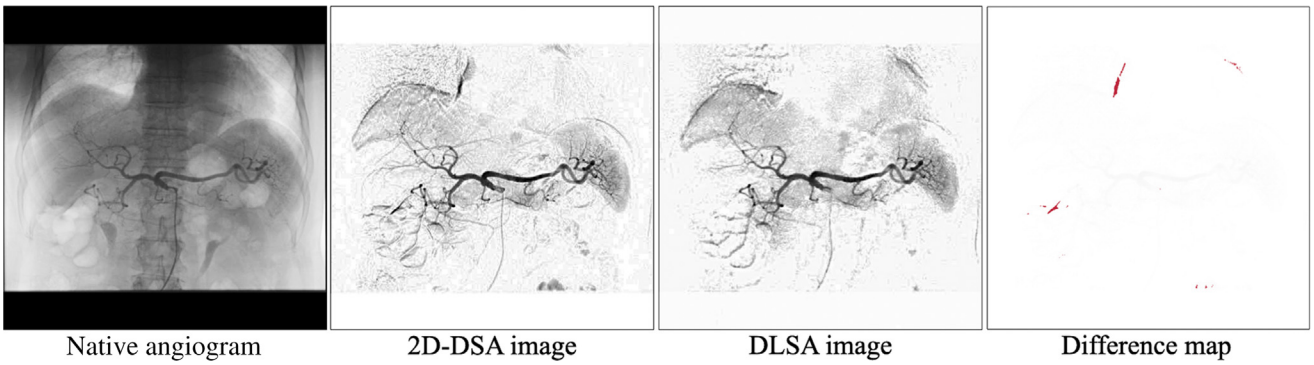

Figure 1. Abdominal angiograms from a man with hepatocellular carcinoma (sequence R): native angiogram, original 2-dimensional digital subtraction angiography (2D-DSA) image, deep learning-based subtraction angiography (DLSA) image, and difference map of the celiac artery from the motion-free test dataset. The peak signal-to-noise ratio and structural similarity of the DLSA image were 43.60 dB and 0.977, respectively. Both the original 2D-DSA and DLSA images provided clinically useful depictions of the main arteries and their branches. Images from the original 2D-DSA and DLSA are highly similar. Differences are shown in red.

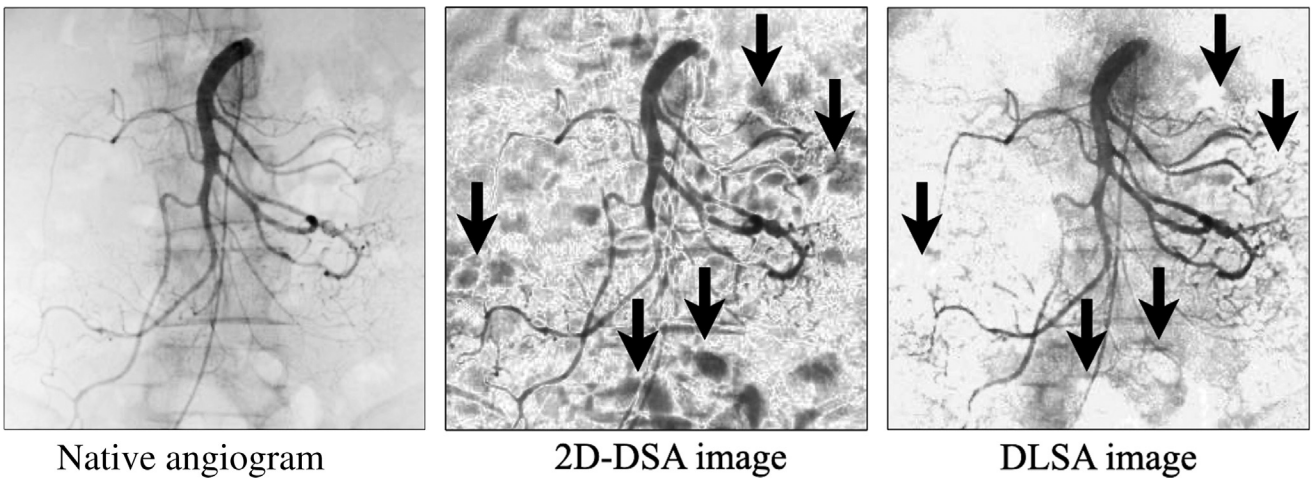

Figure 2. Abdominal angiograms from a man with small bowel hemorrhage prior to treatment (sequence A): these figures show the native angiogram, original 2-dimensional digital subtraction angiography (2D-DSA) image, and deep learning-based subtraction angiography (DLSA) image of the superior mesenteric artery from the motion-artifact test dataset. The mean visual score (± standard deviation) in the vascular visualization test was high, 4.1 ± 0.8 (out of 5). The mean scores in the artifact-reduction test and clinical usefulness test were 4.3 ± 0.9 (out of 5) and 4.3 ± 0.6 (out of 5), respectively. The branches of the jejunal artery overlapped by artifacts of the small intestine in the 2D-DSA image are well described in the DLSA image (arrows).

the paucity of images in the training and validation datasets.

In summary, a DL model was developed to generate synthetic subtraction angiograms without motion artifacts (DLSA images). In qualitative and quantitative evaluations, the DLSA images were similar to or better than 2D-DSA images. The DL model has the potential to replace 2D-DSA in abdominal angiography in cases with motion artifacts. This model does not require any specialized knowledge or skills, and DLSA images in their original resolution can be created with almost no time lag by using existing devices. The trained model is open source (18) and can be used worldwide as well as for research, under the Berkeley Software Distribution license. Therefore, this model has the potential to support interventional radiologists and other image-guided therapy specialists with their patients.

ACKNOWLEDGMENTS

The authors thank Mitsuhiro Inomata and Yoshikazu Hashimoto for technical assistance in regard to deep learning. This work was supported by a grant from JSPS KAKENHI (grant number JP20K16769). The funder played no role in the study design, data collection, data analysis, data interpretation, or writing of the report. The corresponding author had full access to all data in the study and the final responsibility of the decision to submit the report for publication.

AUTHOR INFORMATION

From the Department of Diagnostic and Interventional Radiology (H.Y., D.U., A.Y., K.K., S.L.W., T.N., K.M., E.S., A.J., Y.M.), Graduate School of Medicine, Osaka City University, Osaka, Japan; Department of Radiology (S.

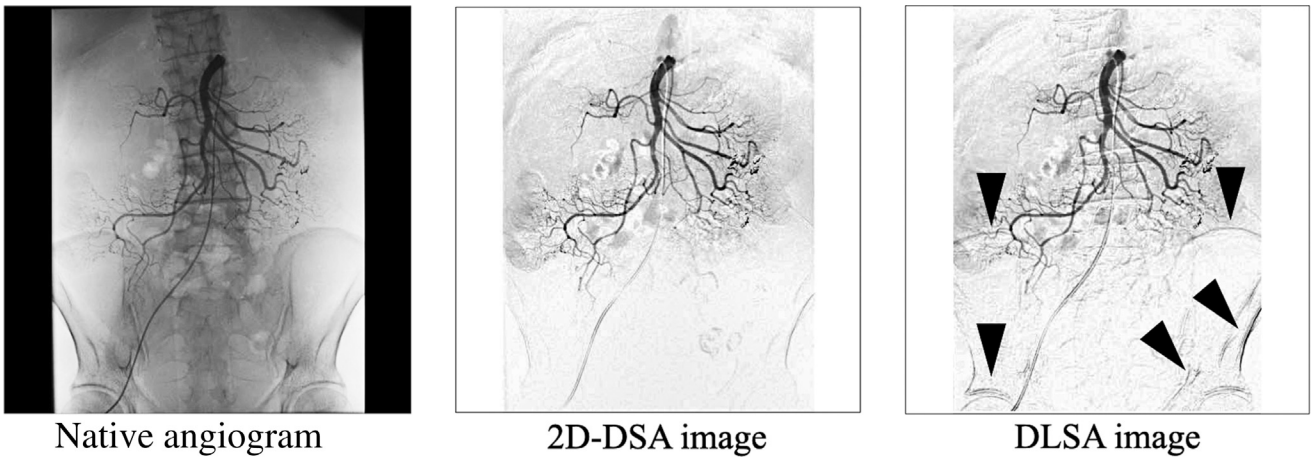

Figure 3. Large-field-of-view abdominal angiograms from a man after coil embolization of small intestinal bleeding (sequence D): native angiogram, 2-dimensional digital subtraction angiography (2D-DSA) image, and deep learning-based subtraction angiography (DLSA) image of the superior mesenteric artery from the motion-artifact test dataset. The mean visual score (± standard deviation) in the vascular visualization test was relatively low, 2.4 ± 1.1 (out of 5). The mean scores in the artifact-reduction test and clinical usefulness test were 2.4 ± 1.1 (out of 5) and 2.4 ± 0.9 (out of 5), respectively. Although every superior mesenteric artery bifurcation was well described in both images, pelvic and femoral bone artifacts were more prominent in the DLSA image (arrowheads).

O.), Osaka Saiseikai Nakatsu Hospital, Osaka, Japan; and Department of Medical Statistics (D.K.), Graduate School of Medicine, Osaka City University, Osaka, Japan. Received April 22, 2021; final revision received January 27, 2022; accepted March 9, 2022. Address correspondence to D.U., Department of Diagnostic and Interventional Radiology, Graduate School of Medicine, Osaka City University, 1-4-3 Asahi-machi, Abeno-ku, Osaka 545-8585, Japan; E-mail: ai.labo.ocu@gmail.com

D.U. reports grants from JSPS KAKENHI during the conduct of the study and grants from LPIXEL Inc. outside the submitted work. Y.M. reports grants and personal fees from Eisai Co., Ltd.; grants from KONICA MINOLTA JAPAN, INC.; grants from Terumo Corporation; grants and personal fees from Bayer Yakuhin, Ltd.; grants and personal fees from Bracco-Eisai Co., Ltd.; grants from Boston Scientific Japan K.K.; grants from Medico's Hirata Inc.; grants and personal fees from DAIICHI SANKYO COMPANY, LIMITED; grants from ASAHI INTECC J-sales, INC.; grants from MEDTRONIC JAPAN CO., LTD.; grants and personal fees from Fuji Pharma Co., Ltd.; grants from Guerbet Japan K.K.; personal fees from Sumitomo Dainippon Pharma Co., Ltd.; personal fees from STELLA PHARMA CORPORATION; personal fees from Siemens Healthcare K.K.; personal fees from Mitsubishi Tanabe Pharma Corporation; personal fees from Novartis Pharma K.K.; and personal fees from Hitachi, Ltd., outside the submitted work. The other authors have not identified a conflict of interest.

REFERENCES

1. Hanafee W, Stout P. Subtraction technic. Radiology 1962; 79:658–661.
2. LeCun Y, Bengio Y, Hinton G. Deep learning. Nature 2015; 521:436–444.
3. Hinton G. Deep learning-a technology with the potential to transform health care. JAMA 2018; 320:1101–1102.
4. Ueda D, Shimazaki A, Miki Y. Technical and clinical overview of deep learning in radiology. Jpn J Radiol 2019; 37:15–33.
5. Levin DC, Schapiro RM, Boxt LM, Dunham L, Harrington DP, Ergun DL. Digital subtraction angiography: principles and pitfalls of image improvement techniques. AJR Am J Roentgenol 1984; 143:447–454.
6. Meijering EH, Niesssen WJ, Viergever MA. Retrospective motion correction in digital subtraction angiography: a review. IEEE Trans Med Imaging 1999; 18:2–21.
7. Lang S, Hoelter P, Schmidt M, et al. Evaluation of an artificial intelligence-based 3D-angiography for visualization of cerebral vasculature. Clin Neuroradiol 2020; 30:705–712.
8. Sundarapandian M, Kalpathi R, Manason VD. DSA image registration using non-uniform MRF model and pivotal control points. Comput Med Imaging Graph 2013; 37:323–336.
9. Ueda D, Katayama Y, Yamamoto A, et al. Deep learning- based angiogram generation model for cerebral angiography without misregistration artifacts. Radiology 2021; 299:675–681.
10. Gao Y, Song Y, Yin X, et al. Deep learning-based digital subtraction angiography image generation. Int J Comput Assist Radiol Surg 2019; 14:1775–1784.
11. Mongan J, Moy L, Kahn CE Jr. Checklist for Artificial Intelligence in Medical Imaging (CLAIM): a guide for authors and reviewers. Radiol Artif Intell 2020; 2:e200029.
12. Cohen JF, Korevaar DA, Altman DG, et al. STARD 2015 guidelines for reporting diagnostic accuracy studies: explanation and elaboration. BMJ Open 2016; 6:e012799.
13. Zhang L, Zhang L, Mou X, Zhang D. FSIM: a feature similarity index for image quality assessment. IEEE Trans Image Process 2011; 20: 2378–2386.
14. Wang Z, Bovik AC, Sheikh HR, Simoncelli EP. Image quality assessment: from error visibility to structural similarity. IEEE Trans Image Process 2004; 13:600–612.
15. Isola P, Zhu JY, Zhou T, Efros AA. Image-to-image translation with conditional adversarial networks. Proceedings of the IEEE Conference on Computer Vision and Pattern Recognition; 2017:1125–1134.
16. Ronneberger O, Fischer P, Brox T. U-net: convolutional networks for biomedical image segmentation. International Conference on Medical Image Computing and Computer-Assisted Intervention. Springer; 2015:234–241.
17. Li C, Wand M. Precomputed real-time texture synthesis with markovian generative adversarial networks. European Conference on Computer Vision. Springer; 2016:702–716.
18. GitHub. Available at: https://github.com/abdominal-dlsa. Accessed April 1, 2020.
19. Paszke A, Gross S, Massa F, et al. PyTorch: an imperative style, high-performance deep learning library. Adv Neural Inf Process Syst 2019; 32:8024–8035.
20. R Core Team. R: a language and environment for statistical computing. Available at: https://www.rproject.org/. Published 2013. Accessed April 1, 2021.
21. Kingma DP, Ba J. Adam: a method for stochastic optimization. ArXiv 2017; arXiv:1412.6980v9.
22. Meijering EH, Niessen WJ, Bakker J, et al. Reduction of patient motion artifacts in digital subtraction angiography: evaluation of a fast and fully automatic technique. Radiology 2001; 219:288–293.

APPENDIX A. METHOD OF CONTRAST MEDIUM ADMINISTRATION

The celiac artery, common hepatic artery, and superior mesenteric artery were selectively catheterized using a 4-F catheter via transfemoral artery access. A nonionic contrast agent (iohexol, Omnipaque-300; GE Healthcare, Boston, Massachusetts) was administered. Undiluted contrast medium was injected from the celiac artery and superior mesenteric artery at 5 mL/s with an injector, and the total volume of contrast injected was 15 mL. From the common hepatic artery, it was injected at 2 mL/s, for the total injection volume of 10 mL.

APPENDIX B. CATEGORY CLASSIFICATION OF MOTION ARTIFACTS

1) Category 1: No artifacts

There are no artifacts in the target vascular region or background region that could affect the treatment.

2) Category 2: Slight artifacts

There are a few artifacts in the target vascular region or background region that would not affect the treatment; therefore, reimaging is not needed.

3) Category 3: Some artifacts and reimaging recommended

There are some artifacts, mainly in the background region, that could affect the treatment, and reimaging is recommended.

4) Category 4: Strong artifacts and reimaging needed

There are strong artifacts in both the target vascular region and background region that could affect the treatment, and reimaging is needed.

APPENDIX C. DETAILED PROCESS FOR MODEL SEARCHING AND HYPERPARAMETER TUNING OF THE DEEP LEARNING MODEL

Various types of deep learning models are available for image-to-image translation. Among these, the pix2pix network was adopted for the deep learning-based subtraction angiography model (1,2). This network can learn the transformational features between paired images using a generative adversarial network. For example, pix2pix is good at extracting features from paired images, such as aerial photographs and maps. The similar relationship between native angiograms and 2D-DSA images without motion artifacts is suitable for feature extraction by pix2pix. The generator network is U-Net, a network that has been successful in semantic segmentation and can use an encoder-decoder system to generate new images (3). By incorporating a skip connection into the encoder-decoder system, the network can learn global features efficiently. The discriminator network employs the PatchGAN, which decomposes the image input to the discriminator into several smaller subregions (4). Each of these regions is then judged as real or fake, and all responses are finally averaged to give the final output of the discriminator. The PatchGAN mechanism allows the discriminator to focus only on local features, while leaving a certain amount of global judgments; therefore, the number of learning parameters can be reduced, resulting in efficient learning.

In this study, the following steps were used to determine the best model and hyperparameters for the final model. As generators, the U-net128-, U-net256-, and ResNet-based models were evaluated. Moreover, the hyperparameters were tuned for the optimizer, learning rate, and batch size. As optimizers, stochastic gradient descent, Adam, and Nadam were evaluated; for the learning rate, the searching range was 0.001–0.05; for the batch size, the search range was 32–256.

Upon completion of the model search and hyperparameter tuning, the final model chosen was U-net256, and the hyperparameters were as follows: (*a*) optimizer, Adam; (*b*) learning ratio, 0.0002; (*c*) momentum parameters, $\beta 1 = 0.5$ and $\beta 2 = 0.999$; and (*d*) batch size, 16.

APPENDIX D. EXPLANATION OF U-NET

U-Net is an encoder-decoder network that consists of convolutional layers without a fully connected layer (3). U-Net introduces an approach called skip connection that concatenates the feature maps output at each layer of the encoder to the corresponding feature maps at each layer of the decoder. With this skip connection, the feature maps in each layer of the encoder can be directly connected to the feature map of the corresponding layer of the decoder, and more detailed features can be represented.

REFERENCES

1. Ueda D, Katayama Y, Yamamoto A, et al. Deep learning-based angiogram generation model for cerebral angiography without misregistration artifacts. Radiology 2021; 299:675–681.
2. Isola P, Zhu JY, Zhou T, Efros AA. Image-to-image translation with conditional adversarial networks. Proceedings of the IEEE Conference on Computer Vision and Pattern Recognition; 2017:1125–1134.
3. Ronneberger O, Fischer P, Brox T. U-net: convolutional networks for biomedical image segmentation. International Conference on Medical Image Computing and Computer-Assisted Intervention. Springer; 2015: 234–241.
4. Li C, Wand M. Precomputed real-time texture synthesis with markovian generative adversarial networks. European Conference on Computer Vision. Springer; 2016:702–716.
5. Wang Z, Bovik AC, Sheikh HR, Simoncelli EP. Image quality assessment: from error visibility to structural similarity. IEEE Trans Image Process 2004; 13:600–612.

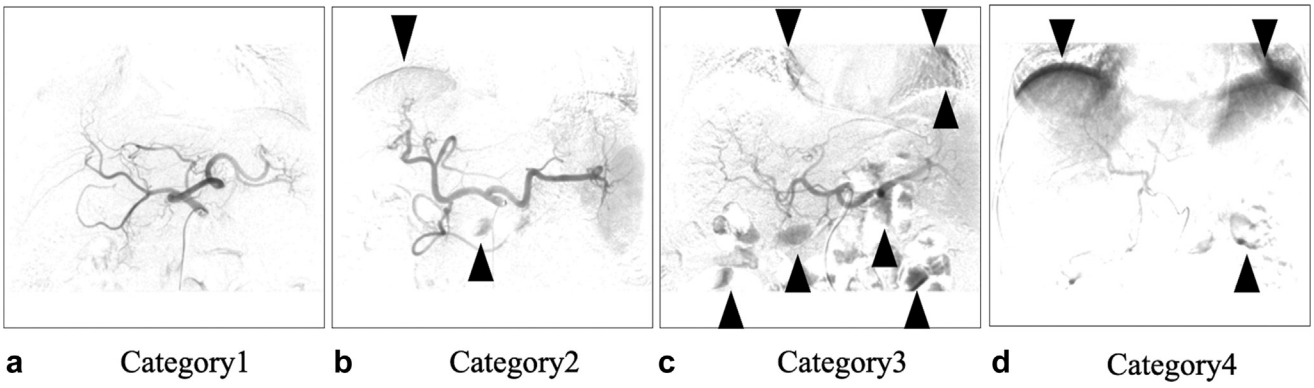

Figure E1. Examples of each classification of motion artifacts. Arrowheads show motion artifacts. **(a)** Category 1: no artifacts. **(b)** Category 2: slight artifacts. **(c)** Category 3: some artifacts and reimaging recommended. **(d)** Category 4: strong artifacts and reimaging needed.

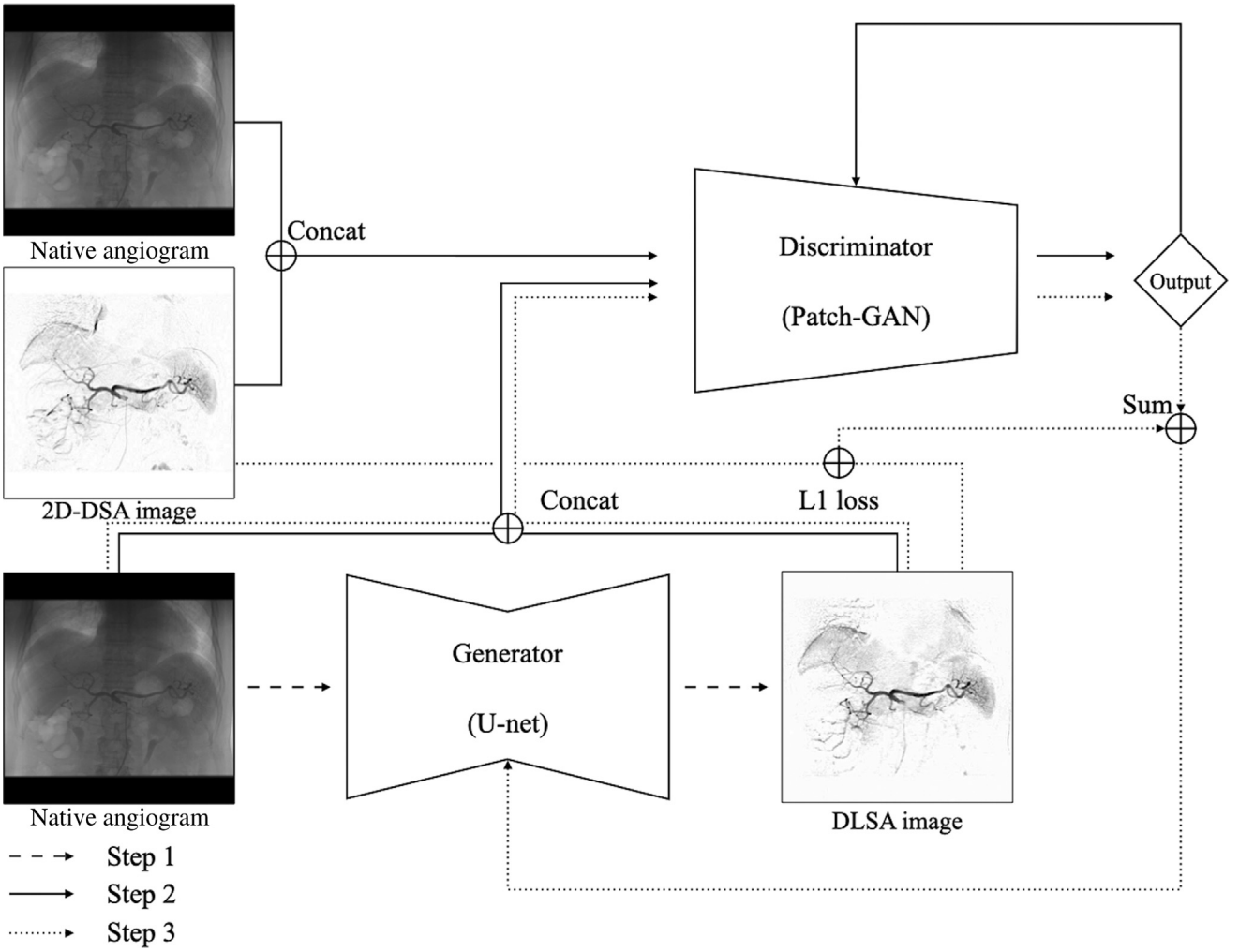

Figure E2. Explanation and overview of the deep learning-based model. Step 1 is an image-generation phase. The generator generates a deep learning-based subtraction angiography (DLSA) image from a native angiogram. The native angiogram is then concatenated with the DLSA image. Step 2 is the learning phase of the discriminator. The concatenated image of a DLSA image and a native angiogram in step 1 or a concatenated image of an original 2-dimensional digital subtraction angiography (2D-DSA) image and a native angiogram from training data are input to the discriminator. The purpose of the discriminator is to correctly classify the DLSA images and 2D-DSA images. Therefore, the loss value is set to be small if the discriminator is correct, whereas it is set to be large if the discriminator is wrong. The resulting discriminator loss value is back-propagated to the discriminator and the parameters are updated. Step 3 is the learning phase of the generator. The purpose of the generator is to generate DLSA images with such a high similarity to 2D-DSA images that they can be mistakenly recognized by the discriminator. Therefore, the loss value is set to be large if the discriminator is correct, whereas it is set to be small if the discriminator is wrong. In addition, the L1 loss values from the original 2D-DSA image and the DLSA image are obtained. These 2 loss values are combined to form the loss value of the generator, and the parameters of the generator are updated. Steps 1 through 3 are repeated as the learning progresses.

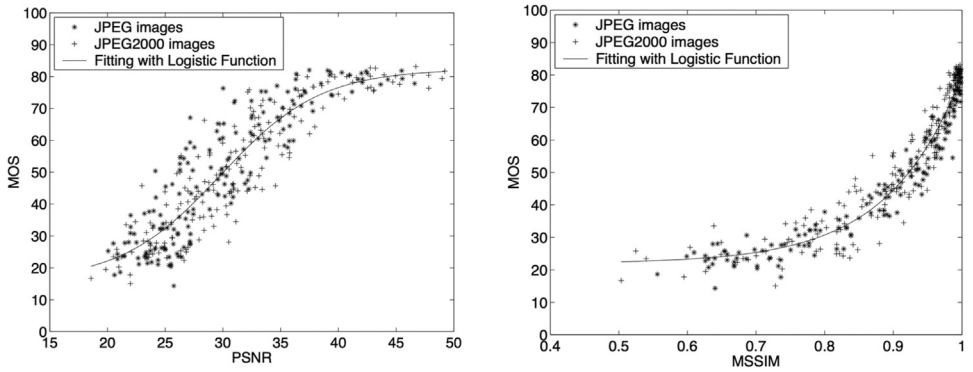

Figure E3. Scatter plots of mean opinion score (MOS) versus model prediction. These figures show the relationships between MOS, peak signal-to-noise ratio (PSNR), and mean structural similarity (MSSIM) (2,5). MOS is a quantitative human judgment of the quality of an event or experience, often on a scale of 0 (bad) to 100 (great). PSNR is an index of image degradation. If the PSNR is above 40, the MOS remains high, indicating a low degree of degradation. SSIM is an index of structural similarity. If the SSIM is 0.8 or higher, the MOS is high, indicating a high degree of similarity.

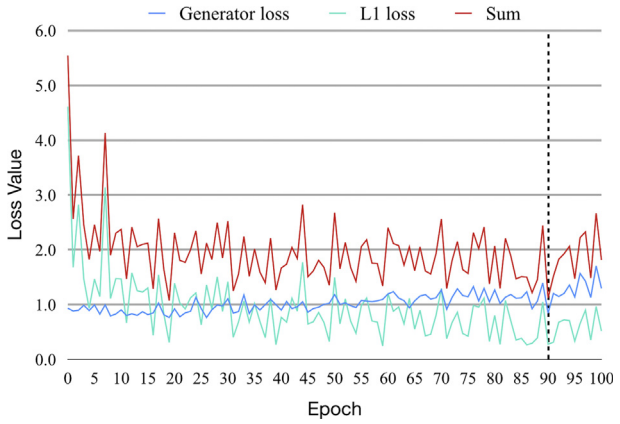

Figure E4. Learning curves for the deep learning model. The vertical axis shows the sum of generator loss and L1 loss, and the horizontal axis shows the number of epochs; the lowest sum of generator loss and L1 loss was 1.119 at 90 epochs.

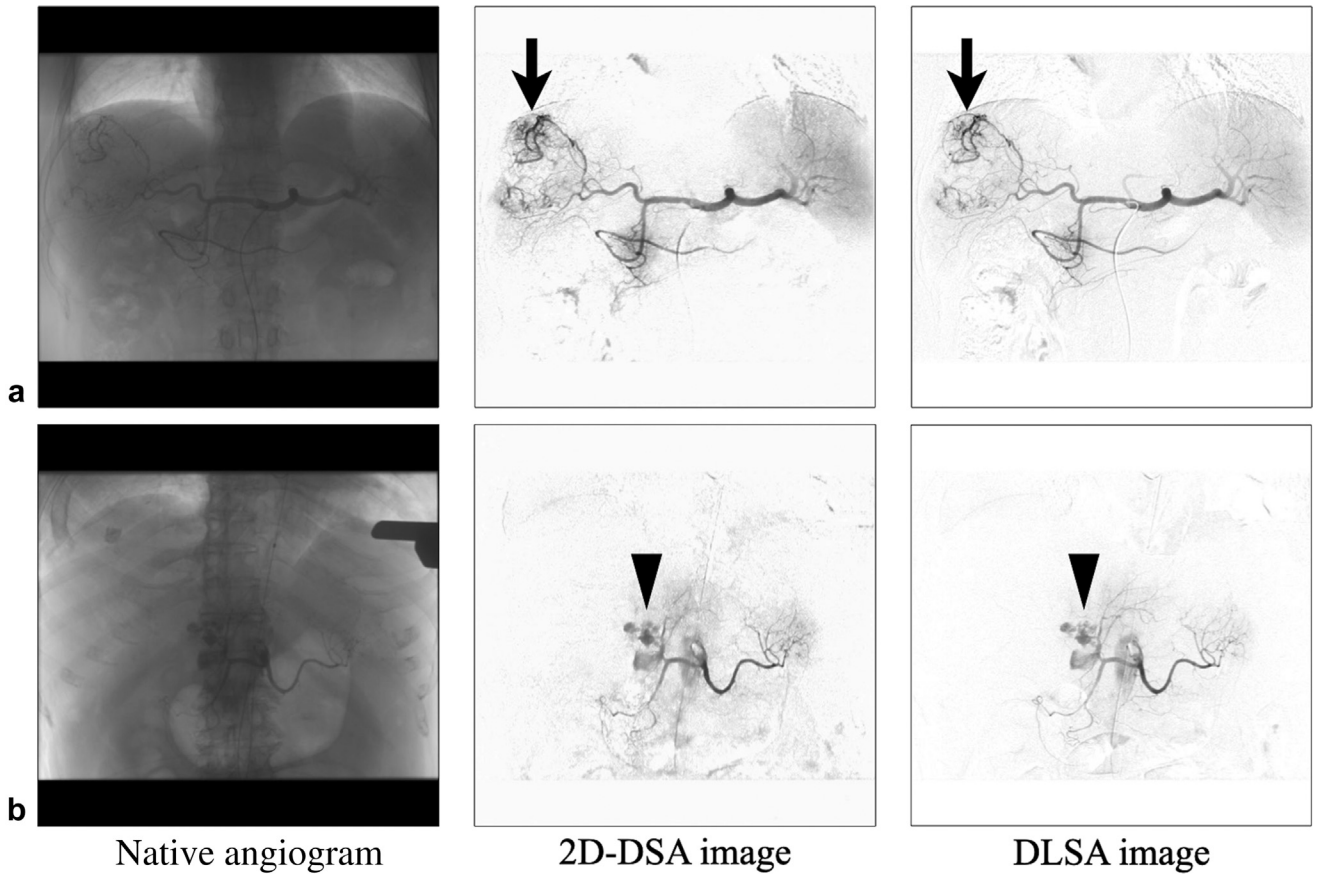

Figure E5. Examples of 2-dimensional digital subtraction angiography (2D-DSA) and deep learning-based subtraction angiography (DLSA) images of hepatocellular carcinoma and bleeding. **(a)** These figures show the native angiogram, original 2D-DSA image, and DLSA image of the celiac artery. These are abdominal angiograms of a man with hepatocellular carcinoma. The arrows show arteries around a hepatocellular carcinoma. **(b)** These figures show the native angiogram, original 2D-DSA image, and DLSA image of the celiac artery. These are abdominal angiograms of a woman with liver injury. The arrowheads show bleeding.

Table E1. Classification of Motion Artifacts

No. of sequences in each category	Training dataset	Validation dataset	Motion-free test dataset	Motion-artifact test dataset
Category 1	78	9	9	0
Category 2	10	2	2	0
Category 3	0	0	0	6
Category 4	0	0	0	4

Table E2. Agreement between the Radiologists' Initial Interpretation on the Classification of Motion Artifacts

	Reader A			
	Category 1	Category 2	Category 3	Category 4
Reader B				
Category 1	93	0	0	0
Category 2	3	14	0	0
Category 3	0	0	6	1
Category 4	0	0	0	3

Note–Values are the number of cases.

Table E3. Classification of Visual Evaluation

Vascular visualization test	
Score	**Description**
1	2D-DSA images are better for visualizing the arteries than DLSA images.
2	2D-DSA images are a little better for visualizing the arteries than DLSA images.
3	The arteries are equally well visualized in both 2D-DSA and DLSA images.
4	DLSA images are a little better for visualizing the arteries than 2D-DSA images.
5	DLSA images are better for visualizing the arteries than 2D-DSA images.
Artifact-reduction test	
Score	**Description**
1	2D-DSA images have very few artifacts compared with DLSA images.
2	2D-DSA images have fewer artifacts compared with DLSA images.
3	The DLSA and 2D-DSA images have the same degree of artifacts.
4	DLSA images have fewer artifacts compared with 2D-DSA images.
5	DLSA images have very few artifacts compared with 2D-DSA images.
Clinical usefulness test	
Score	**Description**
1	2D-DSA images are more useful for guiding the procedure than DLSA images.
2	2D-DSA images are slightly more useful for guiding the procedure than DLSA images.
3	2D-DSA and DLSA images are equally useful for guiding the procedure.
4	DLSA images are slightly more useful for guiding the procedure than 2D-DSA images.
5	DLSA images are more useful for guiding the procedure than 2D-DSA images.

2D-DSA = 2-dimensional digital subtraction angiography; DLSA = deep learning-based subtraction angiography.

Table E4. Vascular Visualization Test using the Visual Assessment with the Motion-Artifact Test Dataset

Sequence	Location	Reader 1	Reader 2	Reader 3	Reader 4	Reader 5	Reader 6	Reader 7	Reader 8	Mean ± SD
A	CA	5/5	3/5	3/5	4/5	5/5	4/5	5/5	4/5	4.1 ± 0.8
B	SMA	3/5	3/5	3/5	2/5	3/5	4/5	3/5	4/5	3.1 ± 0.6
C	CA	3/5	3/5	3/5	4/5	3/5	3/5	5/5	4/5	3.5 ± 0.7
D	SMA	2/5	3/5	3/5	4/5	3/5	2/5	1/5	1/5	2.4 ± 1.1
E	CA	3/5	3/5	2/5	2/5	3/5	3/5	3/5	1/5	2.5 ± 0.7
F	CA	4/5	3/5	3/5	3/5	3/5	3/5	3/5	2/5	3.0 ± 0.4
G	CA	5/5	3/5	3/5	4/5	4/5	4/5	5/5	3/5	3.9 ± 0.7
H	CHA	2/5	1/5	2/5	3/5	2/5	3/5	1/5	2/5	2.0 ± 0.8
I	CA	3/5	3/5	3/5	3/5	3/5	4/5	3/5	3/5	3.1 ± 0.4
J	SMA	2/5	3/5	3/5	4/5	3/5	3/5	3/5	3/5	3.0 ± 0.4

Note–Location refers to the main focus of the angiogram.
CA = celiac artery; CHA = common hepatic artery; SD = standard deviation; SMA = superior mesenteric artery.

Table E5. Artifact-Reduction Test using the Visual Assessment with the Motion-Artifact Test Dataset

Sequence	Location	Reader 1	Reader 2	Reader 3	Reader 4	Reader 5	Reader 6	Reader 7	Reader 8	Mean ± SD
A	CA	5/5	5/5	4/5	3/5	5/5	3/5	5/5	5/5	4.3 ± 0.9
B	SMA	5/5	5/5	4/5	4/5	4/5	3/5	5/5	4/5	4.2 ± 0.6
C	CA	5/5	4/5	4/5	4/5	5/5	3/5	5/5	5/5	4.4 ± 0.7
D	SMA	2/5	2/5	2/5	4/5	2/5	3/5	1/5	2/5	2.2 ± 0.9
E	CA	2/5	2/5	2/5	4/5	2/5	3/5	1/5	2/5	2.2 ± 0.9
F	CA	4/5	3/5	3/5	4/5	3/5	3/5	3/5	2/5	3.1 ± 0.5
G	CA	5/5	5/5	4/5	4/5	4/5	4/5	5/5	3/5	4.3 ± 0.6
H	CHA	5/5	5/5	4/5	4/5	4/5	2/5	5/5	5/5	4.3 ± 1.0
I	CA	4/5	5/5	4/5	4/5	4/5	3/5	5/5	5/5	4.3 ± 0.7
J	SMA	4/5	2/5	2/5	4/5	3/5	3/5	3/5	3/5	3.0 ± 0.6

Note–Location refers to the main focus of the angiogram.
CA = celiac artery; CHA = common hepatic artery; SD = standard deviation; SMA = superior mesenteric artery.

Table E6. Clinical Usefulness Test using the Visual Assessment with the Motion-Artifact Test Dataset

Sequence	Location	Reader 1	Reader 2	Reader 3	Reader 4	Reader 5	Reader 6	Reader 7	Reader 8	Mean ± SD
A	CA	5/5	5/5	4/5	4/5	4/5	3/5	5/5	4/5	4.3 ± 0.6
B	SMA	3/5	5/5	3/5	3/5	3/5	3/5	3/5	5/5	3.5 ± 0.9
C	CA	4/5	4/5	3/5	2/5	4/5	3/5	5/5	4/5	3.6 ± 0.9
D	SMA	2/5	3/5	3/5	3/5	3/5	3/5	1/5	1/5	2.4 ± 0.9
E	CA	3/5	3/5	3/5	3/5	3/5	3/5	1/5	2/5	2.6 ± 0.7
F	CA	4/5	2/5	2/5	4/5	3/5	3/5	3/5	2/5	2.9 ± 0.7
G	CA	5/5	4/5	4/5	5/5	5/5	4/5	5/5	3/5	4.4 ± 0.7
H	CHA	3/5	1/5	1/5	3/5	3/5	2/5	1/5	2/5	2.0 ± 0.8
I	CA	3/5	3/5	3/5	3/5	3/5	3/5	3/5	3/5	3.0 ± 0.0
J	SMA	2/5	2/5	2/5	4/5	3/5	3/5	3/5	3/5	2.8 ± 0.6

Note–Location refers to the main focus of the angiogram.
CA = celiac artery; CHA = common hepatic artery; SD = standard deviation; SMA = superior mesenteric artery.

Table E7. Vascular Visualization Test using the Visual Assessment with the Motion-Free Test Dataset

Sequence	Location	Reader 1	Reader 2	Reader 3	Reader 4	Reader 5	Reader 6	Reader 7	Reader 8	Mean ± SD
K	CA	5/5	3/5	3/5	4/5	3/5	3/5	3/5	3/5	3.4 ± 0.4
L	CA	3/5	3/5	3/5	3/5	2/5	3/5	3/5	4/5	3.0 ± 0.5
M	SMA	4/5	5/5	3/5	4/5	3/5	5/5	3/5	5/5	4.0 ± 0.9
N	CA	2/5	3/5	3/5	4/5	5/5	4/5	5/5	3/5	3.6 ± 0.8
O	CA	3/5	3/5	3/5	3/5	4/5	4/5	3/5	4/5	3.4 ± 0.5
P	CA	4/5	3/5	3/5	3/5	4/5	4/5	3/5	4/5	3.5 ± 0.5
Q	CHA	3/5	3/5	3/5	3/5	4/5	4/5	3/5	3/5	3.3 ± 0.5
R	CA	3/5	3/5	3/5	4/5	5/5	4/5	3/5	4/5	3.6 ± 0.7
S	CA	2/5	3/5	3/5	4/5	3/5	5/5	4/5	5/5	3.6 ± 0.8
T	CA	4/5	3/5	4/5	3/5	5/5	4/5	4/5	5/5	4.0 ± 0.8
U	CA	2/5	3/5	3/5	2/5	2/5	3/5	3/5	3/5	2.6 ± 0.5

Note–Location refers to the main focus of the angiogram.
CA = celiac artery; CHA = common hepatic artery; SD = standard deviation; SMA = superior mesenteric artery.

Table E8. Artifact-Reduction Test using the Visual Assessment with the Motion-Free Test Dataset

Sequence	Location	Reader 1	Reader 2	Reader 3	Reader 4	Reader 5	Reader 6	Reader 7	Reader 8	Mean ± SD
K	CA	5/5	3/5	3/5	4/5	5/5	3/5	5/5	5/5	4.1 ± 0.9
L	CA	5/5	3/5	4/5	4/5	4/5	3/5	5/5	4/5	4.0 ± 0.6
M	SMA	3/5	3/5	3/5	4/5	3/5	5/5	3/5	3/5	3.4 ± 0.7
N	CA	5/5	5/5	4/5	4/5	5/5	4/5	5/5	3/5	4.4 ± 0.7
O	CA	4/5	5/5	3/5	4/5	5/5	3/5	5/5	5/5	4.3 ± 0.9
P	CA	5/5	5/5	3/5	4/5	4/5	4/5	5/5	3/5	4.1 ± 0.8
Q	CHA	3/5	3/5	3/5	4/5	4/5	4/5	3/5	4/5	3.5 ± 0.5
R	CA	5/5	5/5	3/5	4/5	5/5	3/5	5/5	3/5	4.1 ± 0.9
S	CA	5/5	2/5	4/5	4/5	4/5	3/5	5/5	5/5	4.0 ± 1.0
T	CA	5/5	5/5	4/5	4/5	5/5	4/5	5/5	5/5	4.6 ± 0.5
U	CA	5/5	4/5	4/5	4/5	4/5	3/5	5/5	4/5	4.1 ± 0.5

Note–Location refers to the main focus of the angiogram.
CA = celiac artery; CHA = common hepatic artery; SD = standard deviation; SMA = superior mesenteric artery.

Table E9. Clinical Usefulness Test using the Visual Assessment with the Motion-Free Test Dataset

Sequence	Location	Reader 1	Reader 2	Reader 3	Reader 4	Reader 5	Reader 6	Reader 7	Reader 8	Mean ± SD
K	CA	4/5	3/5	1/5	4/5	3/5	3/5	3/5	3/5	3.0 ± 0.8
L	CA	4/5	3/5	3/5	4/5	3/5	3/5	3/5	4/5	3.4 ± 0.5
M	SMA	4/5	5/5	5/5	4/5	3/5	4/5	3/5	4/5	4.0 ± 0.8
N	CA	3/5	3/5	2/5	4/5	5/5	4/5	4/5	3/5	3.5 ± 0.9
O	CA	3/5	4/5	3/5	4/5	3/5	3/5	4/5	4/5	3.5 ± 0.5
P	CA	4/5	3/5	3/5	3/5	4/5	4/5	4/5	4/5	3.6 ± 0.5
Q	CHA	3/5	3/5	2/5	3/5	4/5	4/5	3/5	3/5	3.1 ± 0.6
R	CA	4/5	3/5	3/5	4/5	4/5	4/5	4/5	4/5	3.8 ± 0.5
S	CA	2/5	2/5	2/5	3/5	3/5	4/5	3/5	5/5	3.0 ± 1.0
T	CA	4/5	4/5	3/5	4/5	5/5	3/5	4/5	5/5	4.0 ± 0.8
U	CA	3/5	3/5	2/5	2/5	3/5	3/5	3/5	4/5	2.9 ± 0.6

Note–Location refers to the main focus of the angiogram.
CA = celiac artery; CHA = common hepatic artery; SD = standard deviation; SMA = superior mesenteric artery.